J Nanopart Res (2014) 16:2526
DOI 10.1007/s11051-014-2526-8

RESEARCH PAPER

Synthesis of silver-titanium dioxide nanocomposites for antimicrobial applications

X. H. Yang · H. T. Fu · X. C. Wang · J. L. Yang · X. C. Jiang · A. B. Yu

Received: 8 April 2014 / Accepted: 16 June 2014 / Published online: 25 July 2014

Abstract Silver-titanium dioxide (Ag-TiO_2) nanostructures have attracted increasing attention because of unique functional properties and potential applications in many areas such as photocatalysis, antibacterial, and self-cleaning coatings. In this study, Ag@TiO_2 core–shell nanostructures and Ag-decorated TiO_2 particles (TiO_2@Ag) (the size of these two nanoparticles is ranging from 200–300 nm) have been synthesized by a developed facile but efficient method. These two types of hybrid nanostructures, characterized by various advanced techniques (TEM, XRD, BET and others), exhibit unique functional properties particularly in antibacterial toward Gram negative *Escherichia coli,* as a case study. Specifically: (i) the TiO_2@Ag nanoparticles are superior in bacterial growth inhibition in standard culture conditions (37 °C incubator) to the Ag@TiO_2 core–shell ones, in which silver may dominate the antibacterial performance; (ii) while after UV irradiation treatment, the Ag@TiO_2 core–shell nanoparticles exhibit better performance in killing grown bacteria than the TiO_2@Ag ones, probably because of the Ag cores facilitating charge separation for TiO_2, and thus produce more hydroxyl radicals on the surface of the TiO_2 particles; and (iii) without UV irradiation, both TiO_2@Ag and Ag@TiO_2 nanostructures show poor capabilities in killing mature bacteria. These findings would be useful for designing hybrid metal oxide nanocomposites with desirable functionalities in bio-applications in terms of sterilization, deodorization, and water purification.

Keywords Silver · Titanium dioxide · Nanocomposites · Antibacterial · Environmental and energy applications

X. H. Yang · H. T. Fu · X. C. Jiang (✉) · A. B. Yu
School of Material Science and Engineering, The University of New South Wales, Sydney, NSW 2052, Australia
e-mail: xcjiang@unsw.edu.au

X. C. Wang · J. L. Yang
Adult Cancer Program, Lowy Cancer Research Centre and Prince of Wales Clinical School, The University of New South Wales, Sydney, NSW 2052, Australia

Introduction

Harmful microorganisms may cause some serious problems to human health such as watery diarrhea to severe dysentery and fever, if they are not controlled properly (Chen et al. 2010; Liga et al. 2013; Mitoraj et al. 2007; Seo et al. 2007). Antibacterial using different methods or materials have been widely studied (Burt 2004; Feng et al. 2000; Marambio-Jones and Hoek 2010; Molan 2006; Pal et al. 2007). Of the achieved so far, titanium dioxide (TiO_2) and silver (Ag) nanoparticles (NPs) have attracted more attention because of cost-saving, stability, and high efficiency, although they have different antibacterial mechanisms. For the TiO_2 particles, the bactericidal property was firstly reported by Matsunaga et al. who

found that the Coenzyme A of microbial cells can be oxidized photo electrochemically with platinum-loaded titanium oxide, leading to the inhibition of respiratory activity and to the death of bacteria (Matsunaga et al. 1985). Specifically, the infiltration and photocatalytic oxidation of TiO_2 NPs can lead to the damage of the plasma membrane and loss of enzymatic activity which result in the metabolic inactivation of the microorganisms (Thabet et al. 2013). The antimicrobial activity of TiO_2 NPs may be strongly dependent on the high surface areas and the enhanced surface electronic effect (Thiel et al. 2007). However, the use of TiO_2 is limited in only absorbing UV light (wavelength < 380 nm) due to its wide bandgap (~ 3.2 eV for bulk anatase TiO_2).

Different from the TiO_2 NPs, Ag NPs can incorporate bacteria surface and intracellular uptake of the bacteria (e.g., *Escherichia coli*, noted as *E. coli*), leading silver to binding with sulfur-containing membranes and cytoplasmic proteins to inactivate bacteria (McDonnell and Russell 1999; Pal et al. 2007). In addition, silver ions (Ag^+) can inhibit phosphate uptake and exchange in *E. coli* and cause efflux of accumulated phosphate, which finally results in cell collapse (Schreurs and Rosenberg 1982). Silver ions may also lead to disorder of DNA replication and detachment of the cytoplasm membrane from the cell wall (Feng et al. 2000; Yamanaka et al. 2005). Silver atoms and ions (Ag^0 and Ag^+) have been found effective antimicrobial performance in wound dressing (Ip et al. 2006), textiles (YeonáLee et al. 2007), bone implants (Schneider et al. 2008), and self-sterilizing (Loher et al. 2008).

In addition, Ag nanoparticles can be found in diverse commercial products, especially food storage materials. However, the cytotoxicity of Ag NPs has caused wide concerns by scientists and engineers in the past (Liu et al. 2011 and relevant references in this paper). In vitro cell line studies have shown decreased mitochondrial function after exposure to Ag NPs in human skin carcinoma cells, hepatoma cells, alveolar epithelial and macrophage cell lines, human epidermal keratinocytes and fibroblasts, human lung fibroblast cells (IMR-90), and glioblastoma cells (U251). Ingestion of Ag can cause agyria, the benign condition characterized by the bluish-graying of the skin that occurs through the preferential deposition of Ag in the basal lamina of soft tissues such as the liver, and spleen and blood vessels, gastrointestinal tract, and kidney. Liu et al. demonstrated that oxidative stress might contribute to Ag NPs cytotoxicity, though the exact mechanism behind Ag NPs toxicity is suggested oxidative stress and lipid peroxidation playing an important role in Ag NPs elicited cell membrane disruption, DNA damage, protein damage, and subsequent cell death; however, to reveal whether apoptosis involved in Ag NPs toxicity, further studies are underway.

Furthermore, although the TiO_2 nanoscale colloids have been widely used in sunscreen for anti-UV irradiation, the potential toxicity of such photo-activated TiO_2 particles on exposure of humans and the environment remains unknown. A good example in this area reported by Petkovic (Petković et al. 2011 and relevant reference in this paper), who studied whether pre-irradiation of TiO_2 particles with UV influences their cytotoxic and genotoxic potential in human hepatoma HepG2 cells. They found that the non-irradiated TiO_2 at 1.0–250 μg/ml did not reduce viability of HepG2 cells, nor induce significant increases in DNA strand breaks; only TiO_2(<25 nm in diameter) induced significant increases in oxidative DNA damage. After UV pre-irradiation, both TiO_2 (<25 nm) and TiO_2 (>100 nm) reduced cell viability and induced significant increases in DNA strand breaks and oxidative DNA damage. That is, UV pre-irradiation of anatase TiO_2 particles results in increased cytotoxic and genotoxic potential. In our study, no human cells but *E. coli* bacteria was tested, and there may be some common toxic mechanisms from Ag or TiO_2 nanoparticles in acting on both human cells and *E. coli* bacteria. However, more work needs to be performed for detailed investigations regarding the biosafety of Ag and TiO_2 nanoparticles.

What will happen for the hybrid TiO_2 and Ag nanostructures, either Ag@TiO_2 core–shell structure or Ag-decorated TiO_2 structure in antibacterial? Our recent studies revealed that for the Ag@TiO_2 core–shell nanocomposites, the photogenerated electron-hole (e^--h^+) pairs could be efficiently separated due to Ag as an electron trap to facilitate charge separation and hence enhance photocatalytic efficiency, with nearly double efficiency compared to the pure TiO_2 NPs and P25 TiO_2 (Wang et al. 2012; Wu and Long 2011). The Ag@TiO_2 core–shell particles may also improve the Ag stability and longevity in antibacterial, however, little reported in the literature. It is also expected that superior antibacterial performance will be delivered by the Ag@TiO_2 core–shell nanostructures to individual TiO_2 or Ag nanoparticles. A number of methods have been

proposed for fabricating Ag-TiO_2 nanocomposites, for example, Ag@TiO_2 core–shell nanoparticles can be prepared by a so-called one-step route using N,N,-Dimethylformamide (DMF) to reduce silver nitrate, and TiO_2 was anchored to the metallic core by hydrolysis of titanium isopropoxide (Zhang et al. 2006). The metal@TiO_2 core–shell nanocomposites can also be obtained by a hydrothermal treatment of TiF_4 and colloidal noble metal particles (Zhang et al. 2011). Isabel et al. reported a nanostructure composed of silver cores and 1–2 nm layer of TiO_2 produced by a simultaneous reduction of silver and condensation of titanium butoxide (Pastoriza-Santos et al. 2000).

In this study, a facile but effective synthesis method will be developed to prepare hybrid Ag-TiO_2 nanostructures under mild conditions. Different from other synthesis methods, this approach can be operated under mild condition ($\leq$100 °C, 2 h). The as-prepared core–shell structures show well coating of TiO_2 on Ag particles, high surface area of TiO_2 layer, mixed anatase, and rutile phases, and have been proved with significantly high photocatalytic property (Yang et al. 2013). The microstructure, composition, and properties will be characterized by various advanced techniques, such as transmission electron microscope (TEM), energy dispersive X-ray spectroscopy, X-ray diffraction (XRD), Brunauer Emmett Teller (BET), and ultraviolet-visible (UV-Vis) spectroscopy. In particular, the novelty of this work is to test and compare the antibacterial ability of Ag@TiO_2 core–shell nanoparticles and Ag-decorated TiO_2 nanoparticles in both bacterial growth inhibition and killing grown bacterial (e.g., *E. coli*). Finally, the antibacterial mechanisms of different Ag-TiO_2 nanostructures and the relationship between structure and antibacterial behavior will be discussed. The significance of these findings is to help developing highly efficient photocatalysts for environmental remediation in terms of antibacterial, deodorisation, and water purification.

Experimental section

Preparation of Ag@TiO_2 core–shell structure

Synthesis of Ag@TiO_2 core–shell structure was conducted, by reference to our recent studies (Yang et al. 2013), but some modifications have been made. In a typical protocol of generating Ag cores, a few steps were involved. First, 10 mL of EG (ethylene glycol) solution containing a small amount of polyvinylpyrrolidone (PVP, 0.050 g) was stirred vigorously until all the PVP dissolved completely and the solution became transparent. 0.02548 g of $AgNO_3$ (0.15 mmol) was dissolved in 5 mL of EG solution, followed by vigorous stirring until the solution became homogeneous. Second, two solutions were put into a 25-mL vial and mixed homogeneously by stirring, followed by placing the vial into a Teflon-lined stainless steel autoclave (50 mL capacity). The autoclave was heated in an oven and maintained at a temperature range of 80–180 °C for different times (30 min to a few hours). The color of the reaction system changed from light yellow to brown. Finally, Ag nanoparticles were collected by centrifuge and washed several times with ethanol and water for further use.

The preparation of Ag@TiO_2 core–shell structures could be demonstrated as below: First, 0.05 mL titanium (IV) butoxide 97% (TBT) was added to 10 mL ethylene glycol (EG). The mixture was magnetically stirred for $\sim$8 h at room temperature, labeled as solution A. Second, 3 mL of 0.01 M Ag colloids suspension was poured into 10 mL acetone under stirring for 5 min, labeled as solution B. Third, 0.5 mL solution A was added into solution B, leaving it for 1 h without disturbance. Some yellow brown precipitates were collected by centrifugation and then refluxed in boiling water for $\sim$2 h. Finally, to get Ag@TiO_2 core–shell powders, the solution was centrifuged at a rate of 3000 rps for 10 min, and the precipitates were washed with alcohol and water several times, followed by drying in an oven at 60 °C for 24 h for further characterizations.

Preparation of TiO_2@Ag surface-doped nanoparticles

TiO_2 colloids were synthesized by following the approach described in our recent study but with some modifications (Yang et al. 2012). To generate Ag-decorated TiO_2 nanostructures with well control, 0.01 mM of TiO_2 colloids was dispersed in 15 mL EG solution and stirred to make sure homogeneously. Then, 0.01 mL of 0.1 M $AgNO_3$ and 60 μL hexylamine were added to the above solution simultaneously, and then left without disturbance at room temperature for 2 h to allow the Ag particles to deposit onto the surface of TiO_2 nanospheres. Finally, the precipitate was collected by centrifugation, washed with ethanol and water for several times, following by oven drying at 60 °C for 6 h.

Characterizations

Various advanced techniques were employed to characterize the as-prepared nanoparticles, including:

(i) Irradiation of the TiO_2/Ag hybrid nanostructure was carried out in a quartz cuvette under UV lamp (NEC, 15 W, 300–400 nm, maximum emission 350 nm, Germany);
(ii) Transmission electron microscopy (TEM) images were conducted with a JEOL1400 operated at an acceleration voltage of 100 kV, in which the specimen was prepared by dropping the particle suspension onto copper grids covered with amorphous carbon and air drying;
(iii) Energy dispersive spectroscopy (EDS) analysis was conducted on an energy dispersive X-ray spectrometer attached to a Philips CM200 emission scanning electron microscope;
(iv) The UV-Vis absorption spectrum was obtained on a CARY 5G UV-visible spectrophotometer (Varian) with a 1 cm quartz cell;
(v) Powder X-ray diffraction (XRD) pattern of the optimized product was recorded on a Philip MPD diffractometer with Cu Kα radiation, the analysis was done by analysis software XRDUSEM;
(vi) X-ray photoemission spectroscopic (XPS) analysis was conducted with a Physical Electronics PHI 5000 Versa probe spectrometer with Al Kα radiation (1486 eV); Analysis of the spectra was conducted using the Physical Electronics Multipak software package; and
(vii) Specific surface area of the samples was measured by N_2 adsorption at 77 K using the BET method (Tristar, Micromeritics); Prior to the measurement, the samples were pretreated at 150 °C under vacuum (VacPrep, Micromeritics) for at least an hour to remove surface-adsorbed moisture and other volatile organic impurities.

Bacterial strains cultivation

Inactivation experiments were performed in pure culture of *E. coli* O157:H7 strains and *E. coli* BJ5183 strains. Both were cultivated in LB medium (10 g L^{-1} tryptone, 5 g L^{-1} yeast extract, and 5 g L^{-1} NaCl) at 37 °C for 8 h. Optical densities and viable cell numbers were periodically measured to observe the growth behaviors of the strains. Viable cell counts were determined by tenfold serial dilution of 1 mL broth culture in phosphate buffer solution (PBS), followed by inoculation of 0.1 mL aliquots on nutrient agar, by incubation of the plates at 37 °C for 24 h prior to colony plate counting.

Growth inhibition

Escherichia coli inoculums were prepared by growing culture in an incubator at 37 °C overnight and 280 rpm in 50 mL LB medium from a single agar plate colony. A measured volume of 2 mL of the culture was transferred into 100 mL fresh LB and further conditioned for 0.5 h at 37 °C and ~280 rpm to prepare the inoculum. For each growth inhibition experiment, 5 mL *E. coli* inoculums was added into 50 mL LB followed by different loadings of nanoparticles. The experiments were performed in triplicate with hourly sampling measured by optical density at 600 nm (OD600) using a UV-Vis spectrophotometer (Hitachi). Two types of control were employed: a growth control without nanoparticles and the nanoparticles control without *E. coli*, of which the latter was served as a reference to obtain the OD600.

Bactericidal test

The bactericidal activities of Ag@TiO_2 or TiO_2@Ag nanocomposites were determined on each strain, respectively. Disinfection efficiencies of the as-prepared samples were determined under various periods of UV light pre-irradiation. After UV pre-irradiation, inactivation of 7Log10 CFU/mL inoculum concentrations was performed by adding 1 mL of 7Log10 CFU/mL bacterial suspensions into 9 mL suspension containing 80 mg/L Ag@TiO_2 core–shell or TiO_2@Ag nanoparticles at 25°C. After 5-min exposure, 1 mL aliquot of treated sample was neutralized in PBS for 3 min. The surviving bacteria population was determined through viable cell counting. All results were presented as an average value of triplicates. The bacterial population survival ratio can be defined as follows:

$$\text{Population survival ratio} = 1 - \frac{\log(A) - \log(B)}{\log(A)} \times 100\,\%,$$

where A is the number of original bacterial population, and B is the number of bacterial population after inactivation process.

Statistical analysis

The quantitative data of antibacterial tests were obtained from triplicate experiments on three samples, shown as mean value ± standard deviation (SD).The difference across groups was analyzed by one-way analysis of variance (ANOVA), followed by a Post-Hoc Bonferroni test. Among the groups, the results were further analyzed by a non-parametric Kruskal–Wallis test, followed by a non-parametric Post-Hoc test. P (two-tailed) < 0.05 was considered as significant. Statistical analyses were performed using IBM SPSS Statistics. 21 (IBM Chicago, IL).

Results and discussion

Particle structure and composition

The structure of nanoparticles was characterized. Figure 1 shows TEM images that the Ag@TiO_2 core–shell nanoparticles have Ag cores with diameters of 50–100 nm generated by a polyol-thermal approach (Fig. 1a) (Jiang et al. 2011b). The TiO_2 colloids were synthesized with mild condition by water boiling titanium glycolate for 1–2 h (Fig. 1b), according to our recent report (Yang et al. 2012). Figure 1c shows the TiO_2-coated Ag nanostructures, generated by a simple TiO_2 coating method (Yang et al. 2013). TiO_2 shell thickness could be tunable from a few to tens nanometers, depending on the ratio of titanium to silver (Jiang et al. 2003). The brownish Ag@TiO_2 powder containing Ag, Ti, and O elements was identified by EDS technique (Fig. 1e). The peaks at 3.2 and 0.7 keV can be assigned to Ag and O element, the peaks at 0.3 and 4.6 keV are assigned to Ti element, while the observed peaks of Cu may be originated from the copper grid used for the TEM observation.

Meanwhile, the nanostructures of TiO_2 surface decorated by Ag colloids (Fig. 1d) were prepared via a developed hexylamine reduction approach, in which the silver nitrate was dispersed in ethylene glycol containing evenly dispersed TiO_2 nanospheres, then reduced by hexylamine and finally the Ag colloids deposited on the surface of TiO_2 nanoparticles. Figure 1d shows that the small silver NPs with size of 3–10 nm (dark dot) deposited on the surface of TiO_2 nanospheres ($\sim$100 nm in diameter). From the EDS spectrum shown in Fig. 1f, an intensive Ag peak compared to that from the Ag@TiO_2 core–shell particles was observed and centered at around 3.2 keV, probably caused by the exposed Ag particles on TiO_2 surface. The elemental Ti and O peaks can also be clearly identified in the EDS spectrum.

XRD analysis

To identify the composition, the XRD technique was applied in this work (Fig. 2). The diffraction peaks centered at 38.12°, 44.3°, 64.4°, and 77.4° can be assigned to Ag (111), (200), (220), and (330) crystal planes of the face-centered-cubic (fcc) silver, respectively. While for those centered at 25.84°, 38.48°, 48.44°, 54.98°, and 63.62° could be assigned to the anatase TiO_2(101), (004), (200), (211), and (204) crystal planes, respectively (Jiang et al. 2003). For the Ag@TiO_2 core–shell nanostructures, the XRD pattern shows combined peaks originated from both Ag and anatase TiO_2 (Fig. 2a). The Ag content in such nanostructures is estimated to 58.4 wt% (Table 1). With careful inspection, the presence of Ag_2O and rutile TiO_2 phase in the Ag@TiO_2 core–shell structures could also be proved by the XRD technique. It was noted that the Ag_2O has been demonstrated to impart additional antimicrobial activity in previous reports (Bellantone et al. 2002; Gunawan et al. 2009; Wang et al. 2009).

Figure 2b shows the XRD pattern of TiO_2@Ag nanoparticles, in which the diffraction peaks positioned at $2\theta = 37.71$, 43.83 , 63.71 , and 76.47° could be assigned to metal silver, whereas the peaks centered at 25.27°, 38.51°, 47.98°, 54.99°, 62.57°, and 74.9° could be assigned to the anatase TiO_2 phase. The Ag content in such nanostructures is estimated to 17.4 wt% (Table 1). Surprisingly, no rutile TiO_2 and Ag_2O were detected and observed in such Ag-decorated TiO_2 nanoparticles. This means that the Ag@TiO_2 core–shell nanostructures are composed of more compositions such as rutile TiO_2 and Ag_2O,

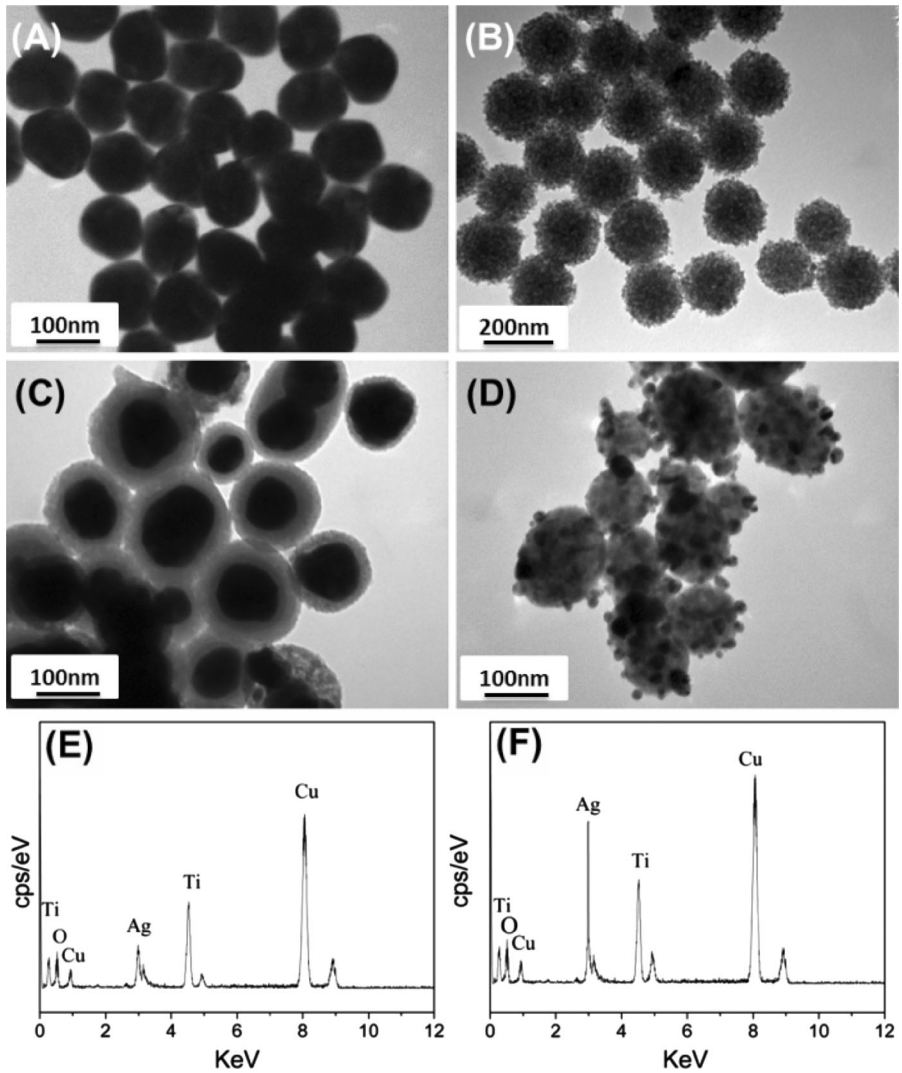

Fig. 1 TEM images of **a** Ag nanoparticles, **b** TiO_2 nanoparticles, **c** Ag@TiO_2 core–shell nanocomposites, **d** TiO_2 surface decorated by Ag nanocomposites, **e** and **f** EDS spectra for **c** and **d** nanocomposites

which may play a role in the photocatalysis, as discussed in our recent work (Yang et al. 2013).

XPS elemental analysis

To make clear, the Ag valence states (Ag^+ or Ag^0) are very helpful for understanding the antimicrobial function. The composition in the Ag@TiO_2 core–shell structure was also investigated by XPS analysis. The characteristic energy spectra consist of five kinds of atoms: titanium (Ti), oxygen (O), silver, a trace amount of carbon (C), and nitrogen (N) in the survey spectrum (Fig. 3a). The existence of C may be ascribed to the adventitious hydrocarbon from the XPS instrument itself. The photoelectron peaks for Ti2p, O1s, and Ag3d were detected and analyzed with binding energies (BE) around 459, 5301, and 3672 eV, respectively.

To further confirm the elemental presence status, the high energy resolution XPS spectra of Ti2p region and O1s region are displayed in Fig. 3b, c, respectively. The peaks for Ti2p appear at 459.6 eV (Ti2p3/2) and 465.4 eV (Ti2p1/2), with slight shifting toward higher binding energies compared to those of the pure anatase TiO_2 (Ti2p3/2= 458.8 eV and Ti2p1/2= 464.8 eV) (Jiang et al. 2011a). This is probably caused by the electrons in Ti–O bond transfer partially to the grain interface between Ag and TiO_2. The shifting of peaks in the high resolution O1s spectra (Fig. 3c) also indicates electrons immigration between

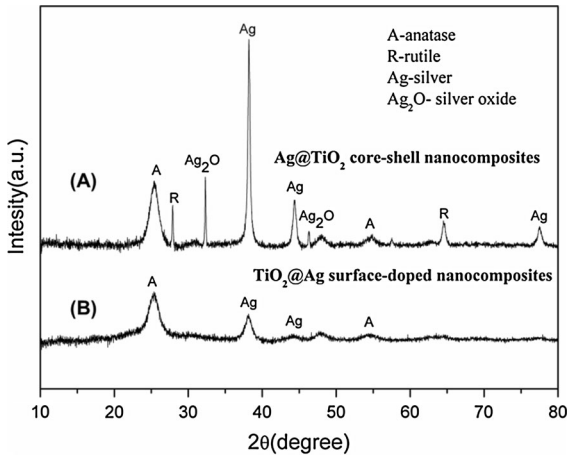

Fig. 2 XRD patterns of the as-prepared $Ag@TiO_2$ core–shell nanocomposites *A* and TiO_2 surface decorated by Ag nanocomposites *B*

Table 1 Comparison of $Ag@TiO_2$ core–shell and $TiO_2@Ag$ surface-doped structures

Nanostructure	Average particle size (nm)	Ag:TiO_2 weight ratio (wt%)	BET surface area (m^2/g)	Pore size (nm)
$Ag@TiO_2$	113	58.4	170	4.9
$TiO_2@Ag$	123	17.4	151	5.4

Ti–O bonds (Orts-Gil et al. 2013). In addition, the binding energies of Ag3d5 peak, 368.3 eV and 367.5 eV were calculated which could be assigned to Ag^0 and Ag_2O (Fig. 3d), respectively. This indicates that the Ag species in the core–shell composites are in the form of Ag and Ag_2O, consistent with the XRD characterizations (Fig. 2a).

Optical property

UV-Vis spectrometer was used to measure the optical properties of nanoparticles. Figure 4 shows the UV-Vis spectra for the as-prepared $Ag@TiO_2$ core–shell structures and TiO_2 surface decorated by Ag nanostructures and Ag nanoparticles (diameter of $\sim$60 nm) which were obtained by a polyol-thermal approach (Jiang et al. 2011a, b), and pure anatase TiO_2 nanoparticles which were prepared by a water boiling method (Yang et al. 2012). The surface plasmon resonance of the Ag nanoparticles centered at $\sim$445 nm (Fig. 4a) weakened when coated with amorphous or anatase TiO_2 nanoparticles, and also shifted in the absorption wavelength region.

For the $Ag@TiO_2$ core–shell particles, the UV-Vis absorption peak is centered at $\sim$320 nm (Fig. 4c), similar to that of pure anatase TiO_2 particles (Fig. 4b). That is, the surface plasmon resonance of Ag nanoparticles is heavily reduced by the surface coated TiO_2. While for those $TiO_2@Ag$ nanostructures, the surface plasmon adsorption intensity of Ag ($\sim$445 nm) dramatically decreased, despite the position is nearly kept, which may be caused by the small size (3–10 nm colloids) or a small ratio in the whole structure. Moreover, a significant blue shift from $\sim$320 to 260 nm occurred for the TiO_2 absorption, when Ag deposited on the surface. However, the real reason is not clear yet at this moment.

BET surface analysis

Surface area or surface-to-volume ratio is critical for the functional properties of nanoparticles, and for their applications in catalysis, gas sensing and those related to contact surfaces. The surface area of the $Ag@TiO_2$ core–shell or Ag-decorated TiO_2 nanostructures may highly affect the antibacterial performance. In this study, the BET surface analysis was conducted. The N_2 adsorption–desorption isotherms and the pore size distribution for $Ag@TiO_2$ core–shell structure are shown in Fig. 5. The isotherms can be ascribed to type IV (BDDT classification), indicating the presence of mesoporous pore structures. The BET surface area of the as-prepared $Ag@TiO_2$ core–shell structure was estimated to $\sim$170 m^2/g, and the average pore size was 4.9 nm. Similar procedures to the Ag-decorated TiO_2 nanostructures were carried out, and the BET surface area was estimated to $\sim$151 m^2/g, with average pore size of 5.4 nm. All the obtained data are listed in Table 1.

Bacterial growth inhibition

The bacterial growth inhibition capability of hybrid TiO_2 and Ag nanostructures was assessed using *E. coli* O157:H7, as a target microorganism. A calibration curve was made at the beginning of growth inhibition test to determine the conversion factor between OD reading at 600 nm and the number of colony forming units growing (per mL) (Fig. 6). Under standard

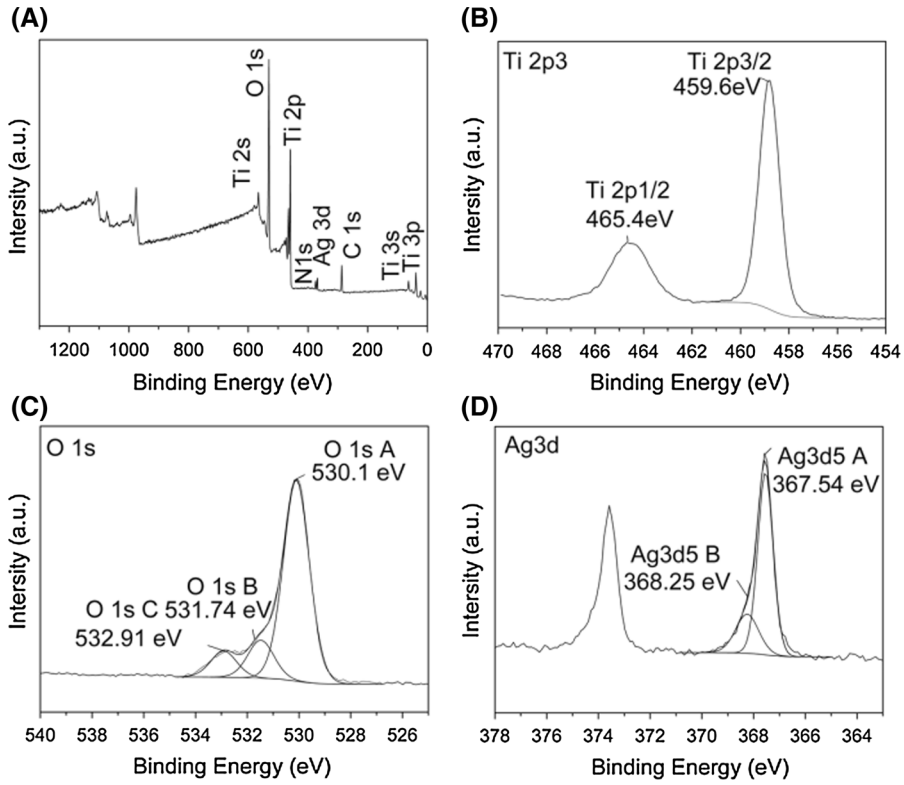

Fig. 3 XPS spectra of $Ag@TiO_2$ core–shell nanocomposites **a** full spectrum and **b–d** spectrum for elemental Ti, O, and Ag, respectively

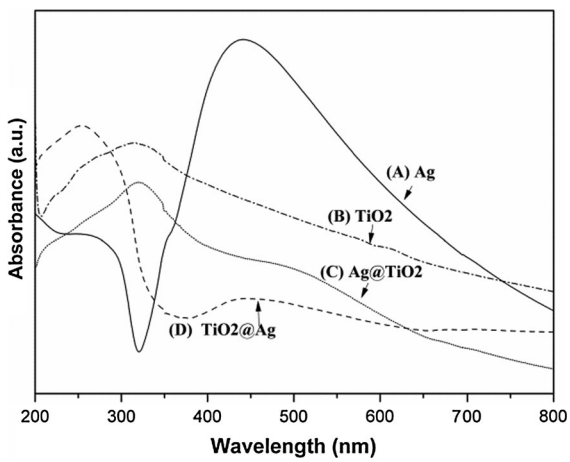

Fig. 4 UV-Vis absorption spectra of Ag nanoparticles *A*, pure anatase TiO_2 nanoparticles *B*, $Ag@TiO_2$ core–shell nanostructures *C*, and TiO_2 surface decorated by Ag nanocomposites *D*, corresponding to those particles shown in Fig. 1**a–d**

operation conditions and in the absence of nanoparticles, *E. coli* growth in Luria Bertani (LB) nutrient media was characterized by a relatively short lag phase of 1 h followed by 3–4 h active log phase before entering stationary phase after 6 h (See Fig. 7 control curve). As expected, the trend of bacterial growth inhibition increases at higher particle loadings. Figure 7 shows the kinetics of *E. coli* growth in the presence of different loadings of the as-prepared $Ag@TiO_2$ core–shell particles. The control trial without any particles was conducted as a reference. The presence of 5 mg/L $Ag@TiO_2$ has a little effect on inhibiting bacterial growth; while at 50 mg/L, a prolonged lag phase was observed. The presence of 100 mg/L of $Ag@TiO_2$ core–shell particles could completely suppress bacterial growth under 6 h. At this stage, the presence of Ag^0 atoms or Ag^+ ions may play an essential role in inhibiting bacterial growth (Gunawan et al. 2009).

In comparison, Ag-decorated TiO_2 nanostructures were tested in the bacterial growth inhibition. Under the same concentration of 80 mg/L, three types of nanoparticles $Ag@TiO_2$, $TiO_2@Ag$, and pure TiO_2 particles were homogenously dispersed into the LB media, respectively. Then the *E. coli* inoculum was transferred into the media suspension for observation.

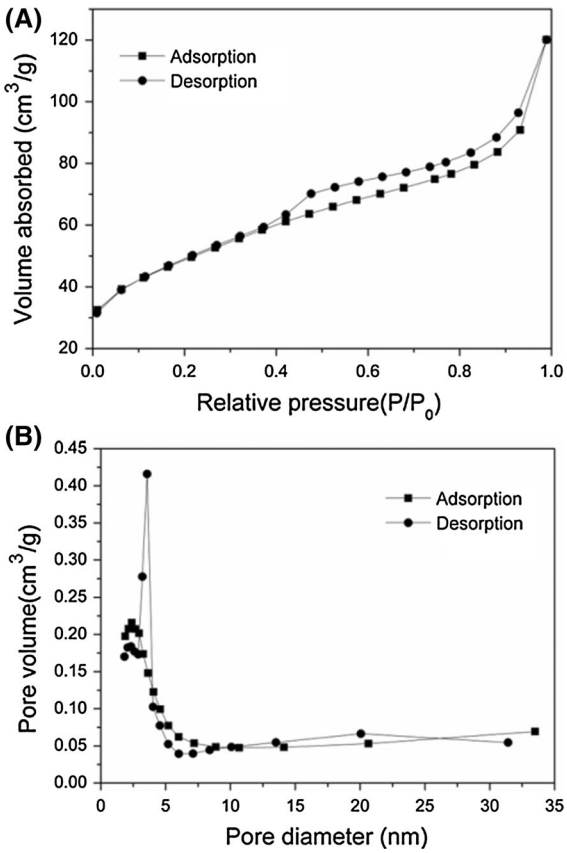

Fig. 5 BET surface area test for $Ag@TiO_2$ core–shell structures showing $S_{Ag@TiO2}= \sim 170.6\ m^2/g$, and average pore size is 4.9 nm

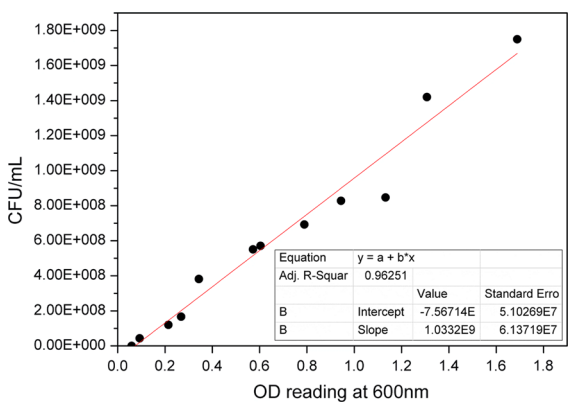

Fig. 6 Calibration curve to calculate the conversion factor between OD reading at 600 nm and the number of colony forming units growing per mL (CFU/mL)

Figure 8 shows the *E. coli* growth trends in the presence of these three kinds of nanoparticles. It was found that the Ag decorated TiO_2 nanostructures show

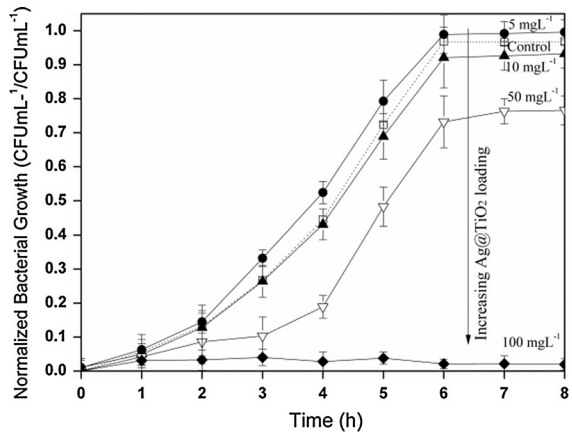

Fig. 7 Kinetic study of *E. coli* growth in Luria Bertani nutrient media at 37 °C in the presence of different loadings of the as-prepared $Ag@TiO_2$ core–shell particles as well as without any particles (control). There were significant differences across the five groups, ($P < 0.001$). 100 mg/L group had a significant difference as compared with any of other four groups ($P \leq 0.015$). There was no significant difference between the other four groups

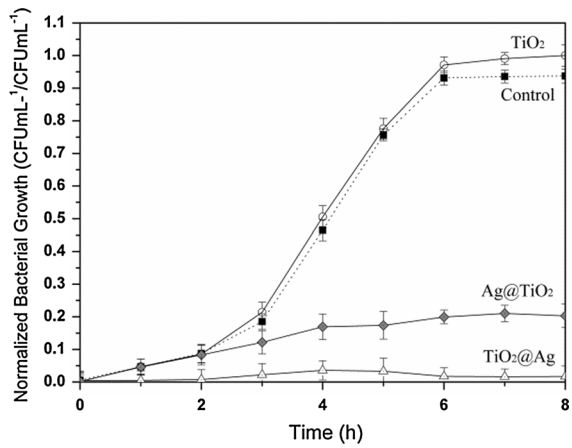

Fig. 8 Kinetic study of *E. coli* growth in Luria Bertani nutrient media at 37 °C in the presence of 80 mg/L of the as-prepared particles as well as a blank. There were significant differences across the five groups, ($P \leq 0.002$). Significant differences were found between $TiO_2@Ag$ and $Ag@TiO_2$ groups ($P = 0.010$), $TiO_2@Ag$ and control ($P = 0.015$), and $TiO_2@Ag$ and TiO_2($P = 0.009$). There was no significant difference between other groups

the most effective performance in bacterial growth inhibition, where no growth indication was observed up to 8 h. The small Ag particles depositing on the surface of TiO_2 support makes it easier to release Ag^+

ions in the aqueous culture media, which consequently contributes to the observed bacterial growth inhibition.

For the Ag@TiO_2 core–shell nanoparticles, the bacteria may grow in the first 2 h, but no active lag phase growth afterward. On the contrary, there was insignificant effect on bacteria growth suppression for the pure TiO_2 nanoparticles, similar to the blank with control. However, the reason why pure TiO_2 has no contribution but Ag-decorated TiO_2 nanostructures can inhibit *E. coli* growth needs to be addressed, as below. Without UV light irradiation, TiO_2 has less photoactivity and generates less electron-hole pairs, and thus weaken performance in *E. coli* growth inhibition, as shown in Fig. 8. While for the Ag@TiO_2 core–shell ones with TiO_2 shells, better inhibition control of *E. coli* growth suggests that it is the silver core nanoparticles that may play a key role in suppressing bacterial growth. The principles underlying antibacterial by silver colloids have been extensively discussed in the literature (Gunawan et al. 2009; Sotiriou and Pratsinis 2010; Xiu et al. 2012). Some researchers demonstrated that the Ag particle size effects on antibacterial activity (Sotiriou and Pratsinis 2010), e.g., for smaller ones (<10 nm), Ag^+ ions easily released, and the antibacterial activity was mainly dominated by Ag^+ ions rather than Ag^0 atoms (Xiu et al. 2012); while for larger Ag ones (>20 nm), the particle itself influenced the antimicrobial activity, despite of less Ag^+ ions released. That is, Ag^+ ions are the definitive molecular toxicant, and the antimicrobial activity could be controlled by modulating Ag^+ ions release. One possible reason for the Ag@TiO_2 core–shell structures to show good performance in growth inhibition is probably that the Ag_2O ($\sim$14%) maybe easy to produce Ag^+ ions. Another reason is the Ag can be used as an electron trap for electrons generated by TiO_2 shell, which may further reduce the possibility of electron-hole recombination, and benefit for generating more ·OH radicals on the core–shell particle surface to inhibit bacterial growth. It needs to point out that the detailed information regarding the relationship between Ag^+ ions release and antibacterial requires more experimental and theoretical work to do in the near future.

Bactericidal assessment

In addition to suppressing bacteria growth from inoculum, antibacterial activities of the as-prepared nanocomposites were also assessed in killing the grown bacteria, when they are in stationary phase. Under dark conditions, the hybrid Ag-decorated TiO_2 nanostructures show poor capability to kill the grown bacteria (Fig. 9). When the concentration of nanocomposites increased to 200 mg/L in aqueous solution, the percentage of survival bacterial population could still be over $\sim$90%.

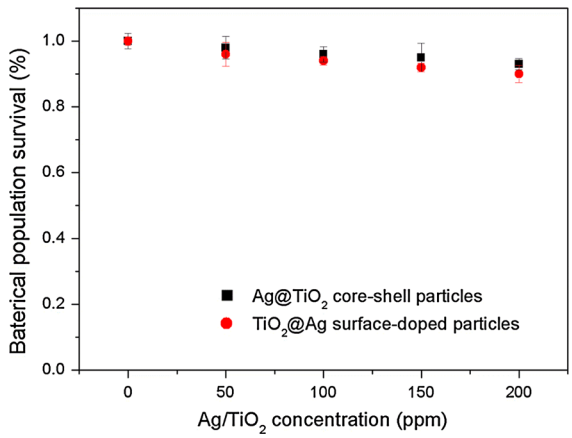

Fig. 9 Dose-dependent growth inhibitory effect of Ag@TiO_2 core–shell particles and the nanostructures of TiO_2 surface decorated by Ag particles on *E. coli* (O157:H7) in dark (UV-free) condition. There were significant differences across two groups ($P \leq 0.012$). *Error bars* correspond to the standard deviation (SD) between three independent measurements

On the contrary, after UV irradiation, both types of nanocomposites Ag@TiO_2 core–shell and Ag-decorated TiO_2 nanostructures exhibited highly enhanced bactericidal activity. Figure 10a shows the survival rate of the grown bacteria population after mixed with nanoparticles at a concentration of 80 mg/L, with different UV irradiation times prior to testing. The cultured *E. coli* O157:H7 was initially diluted with LB media to an optical density of 0.05 at 600 nm, about 10^7 colony forming units (CFU)/mL. The survival of *E. coli* was estimated by a plate count method. It was found, for the UV irradiated pure TiO_2 particles for 240 min, a minimal effect was observed on bacteria inactivation, where >80% bacteria still survived.

Moreover, the UV irradiated Ag@TiO_2 core–shell and Ag-decorated TiO_2 nanostructures exhibited stronger killing bacteria capacities, related closely to irradiation time. For those Ag-decorated TiO_2 surface nanostructures, the bacteria inactivation performance gradually increased with increasing the UV irradiation

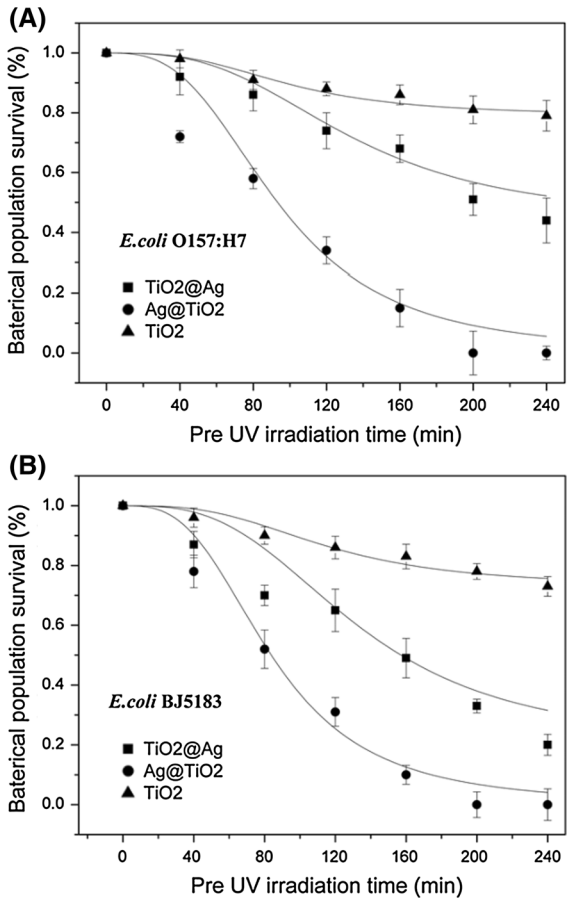

Fig. 10 **a** *E. coli* O157:H7 and **b** *E. coli* BJ5183 inactivation by pure TiO_2 particles, Ag@TiO_2 core–shell particles and the nanostructures of TiO_2 surface decorated by Ag particles under different UV irradiation times. There were significant differences across three groups ($P \leq 0.036$). No significant differences were found between Ag@TiO_2 and TiO_2 ($P = 0.042$). There was no significant difference between other groups. **b** There were significant differences across three groups ($P \leq 0.050$), while insignificant difference between Ag@TiO_2 and TiO_2 ($P = 0.018$) was found. There were no significant differences between other groups

time, e.g., bacterial killing 20 % and 50 % after 120-min and 240-min irradiation, respectively. The bactericidal activities of the Ag@TiO_2 core–shell particles were remarkably enhanced under the same conditions. After 240-min UV irradiation, they can kill more than 90 % *E. coli* O157:H7. As a further confirmation, *E. coli* BJ5183, another strain of *E. coli*, was employed to repeat the assessment (Fig. 10b), and similar results in killing bacterial were confirmed. That is, the bacterial killing capabilities are in the following order: Ag@TiO_2 (core–shell) > TiO_2@Ag (surface decorated with Ag) > pure TiO_2.

To well understand the bactericidal performance, Scheme 1 was used to illustrate the working principles of hybrid silver-titania nanostructures toward bacteria inactivation. For the Ag@TiO_2 core–shell nanostructures, the ground-state electrons at the valence band (VB) are excited to the conduction band (CB) under UV irradiation. Then the CB electrons subsequently migrate to the Ag in a typical Schottky-type mechanism, and the Ag cores attract more electrons from TiO_2 (Chuang and Chen 2009). The holes generated at the valence band react with water molecules to produce hydroxyl radicals (OH·), and partial electrons may also transfer to the adsorbed oxygen on particle surface to produce superoxide anions ($\bullet O_2$). In addition, Ag cores may release some silver ions in this structure due to the formation of Ag_2O. All these factors will benefit for the bacterial inactivation. On the contrary, for UV irradiated TiO_2 surface decorated by Ag nanostructures, the circumstance is a little complicated, because the surface plasmon resonance of silver leads hot electrons to transferring to the TiO_2 (Cushing et al. 2012), while the newly formed Ag^+ ions on TiO_2 surface may accept photogenerated electrons from TiO_2 to be reduced to Ag^0.

Based on the above analysis, it can be assumed that the hydroxyl radicals (OH·) and superoxide anion ($\cdot O_2$) play a crucial role in the antibacterial activity than the Ag^0 and Ag^+ ions under UV irradiation. Under the same conditions, more OH· and $\cdot O_2$ radicals were produced in the Ag@TiO_2 core–shell structures than in the Ag-decorated TiO_2 surface nanostructures, leading to an enhanced performance in killing bacteria.

Conclusions

In this study, we have demonstrated facile but effective methods to prepare hybrid Ag-TiO_2 nanocomposites: Ag@TiO_2 core–shell and Ag-decorated TiO_2 surface nanostructures. They exhibit different capabilities in antimicrobial (i) without UV irradiation, the Ag-decorated TiO_2 surface nanoparticles show superior capability in bacterial growth inhibition to Ag@TiO_2 core–shell ones or pure anatase TiO_2 particles, in which Ag^0 and Ag^+ ions generated on TiO_2 surface play a key role in antimicrobial; (ii)

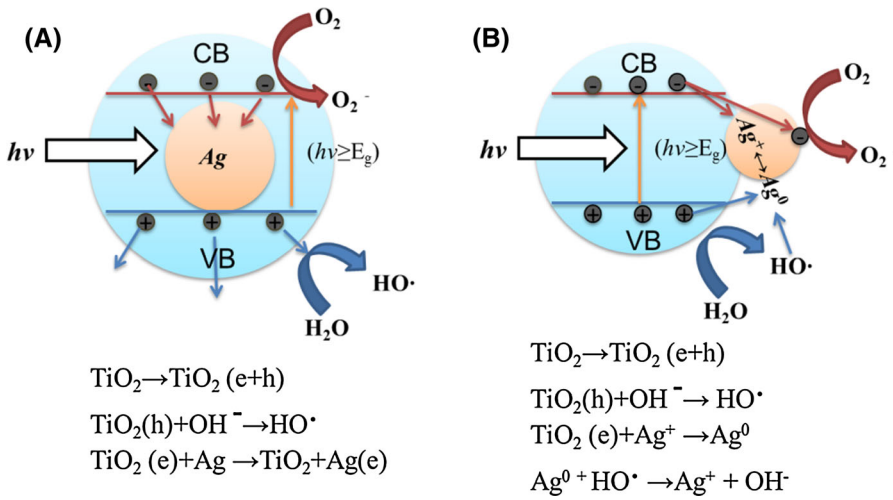

Scheme 1 Illustrating the working species toward microbe inactivation of **a** Ag@TiO_2 core–shell nanoparticles, and **b** Ag-decorated TiO_2 nanoparticles under UV light irradiation

under UV light irradiation, the Ag@TiO_2 core–shell nanocomposites exhibit superior bactericidal performance to others, because Ag cores tend to facilitate charge separation for the photogenerated TiO_2, and hence produce more hydroxyl radicals (OH·) and superoxide anion ($\cdot O_2$) that play a critical role in antibacterial activity; and (iii) two types of bacteria, *E. coli* O157:H7 and *E. coli* BJ5183 were tested and assessed in antibacterial behavior, and the similar trend was found for both Ag@TiO_2 core–shell and Ag-decorated TiO_2 nanostructures. However, we need to point out that the quantitative information regarding the relationship between the produced hydroxyl radicals (OH·) and survival bacterial, and the released Ag^+ ions from Ag cores or Ag_2O and their impact on the antibacterial activities need to be further investigated, experimentally and theoretically. These findings would be useful for design and construction of antibacterial nanomaterials with a high efficiency. This study may open a new path to generate hybrid metal and metal oxide nanostructures with superior functionalities for energy and environmental applications.

Acknowledgments We gratefully acknowledge the financial support of the Australia Research Council (ARC) projects. The authors acknowledge the access to the UNSW node of the Australian Microscopy & Microanalysis Research Facility (AMMRF).

Funding Funding is from financial support of the Australia Research Council (ARC) projects.

Conflict of interest The authors declare no competing financial interest.

References

Bellantone M, Williams HD, Hench LL (2002) Broad-spectrum bactericidal activity of Ag2O-doped bioactive glass. Antimicrob Agents Chemother 46:1940–1945

Burt S (2004) Essential oils: their antibacterial properties and potential applications in foods—a review. Int J Food Microbiol 94:223–253

Chen SF, Li JP, Qian K, Xu WP, Lu Y, Huang WX, Yu SH (2010) Large scale photochemical synthesis of M@ TiO2 nanocomposites (M= Ag, Pd, Au, Pt) and their optical properties, CO oxidation performance, and antibacterial effect. Nano Res 3:244–255

Chuang H-Y, Chen D-H (2009) Fabrication and photocatalytic activities in visible and UV light regions of Ag@ TiO2 and NiAg@ TiO2 nanoparticles. Nanotechnology 20:105704

Cushing SK et al (2012) Photocatalytic activity enhanced by plasmonic resonant energy transfer from metal to semiconductor. J Am Chem Soc 134:15033–15041

Feng Q, Wu J, Chen G, Cui F, Kim T, Kim J (2000) A mechanistic study of the antibacterial effect of silver ions on *Escherichia coli* and *Staphylococcus aureus*. J Biomed Mater Res 52:662–668

Gunawan C, Teoh WY, Marquis CP, Lifia J, Amal R (2009) Reversible antimicrobial photoswitching in nanosilver. Small 5:341–344

Ip M, Lui SL, Poon VK, Lung I, Burd A (2006) Antimicrobial activities of silver dressings: an in vitro comparison. J Med Microbiol 55:59–63

Jiang X, Herricks T, Xia Y (2003) Monodispersed spherical colloids of titania: Synthesis, characterization, and crystallization. Adv Mater 15:1205–1209

Jiang X, Xiong S, Chen C, Chen W, Yu A (2011a) Polyol-thermal synthesis of silver nanowires for Hg^{2+} sensing

detection. J Nanopart Res 13:5087–5101. doi:10.1007/s11051-011-0489-6

Jiang XC, Xiong SX, Tian ZA, Chen CY, Chen WM, Yu AB (2011b) Twinned structure and growth of v-shaped silver nanowires generated by a polyol−thermal approach. J Phys Chem C 115:1800–1810. doi:10.1021/jp110538g

Liga MV, Maguire-Boyle SJ, Jafry HR, Barron AR, Li Q (2013) Silica decorated TiO_2 for virus inactivation in drinking water-simple synthesis method and mechanisms of enhanced inactivation kinetics. Environ Sci Technol 47(12):6463–6470

Liu P, Guan R, Ye X, Jiang J, Liu M, Huang G, Chen X (2011) Toxicity of nano- and micro-sized silver particles in human hepatocyte cell line L02. J Phys: Conf Ser 304:012036

Loher S, Schneider OD, Maienfisch T, Bokorny S, Stark WJ (2008) Micro-organism-triggered release of silver nanoparticles from biodegradable oxide carriers allows preparation of self-sterilizing polymer surfaces. Small 4:824–832

Marambio-Jones C, Hoek EM (2010) A review of the antibacterial effects of silver nanomaterials and potential implications for human health and the environment. J Nanopart Res 12:1531–1551

Matsunaga T, Tomoda R, Nakajima T, Wake H (1985) Photoelectrochemical sterilization of microbial cells by semiconductor powders. FEMS Microbiol Lett 29:211–214

McDonnell G, Russell AD (1999) Antiseptics and disinfectants: activity, action, and resistance. Clin Microbiol Rev 12:147–179

Mitoraj D, Jańczyk A, Strus M, Kisch H, Stochel G, Heczko PB, Macyk W (2007) Visible light inactivation of bacteria and fungi by modified titanium dioxide. Photochem Photobiol Sci 6:642–648

Molan PC (2006) The antibacterial activity of honey: 1. The nature of the antibacterial activity

Orts-Gil G et al (2013) On the role of surface composition and curvature on biointerface formation and colloidal stability of nanoparticles in a protein-rich model system. Colloids Surf B Biointerfaces 108:110–119. doi:10.1016/j.colsurfb.2013.02.027

Pal S, Tak YK, Song JM (2007) Does the antibacterial activity of silver nanoparticles depend on the shape of the nanoparticle? A study of the gram-negative bacterium *Escherichia coli*. Appl Environ Microbiol 73:1712–1720

Pastoriza-Santos I, Koktysh DS, Mamedov AA, Giersig M, Kotov NA, Liz-Marzán LM (2000) One-pot synthesis of Ag@TiO_2 core−shell nanoparticles and their layer-by-layer assembly. Langmuir 16:2731–2735. doi:10.1021/la991212g

Petković J, Küzma T, Rade K, Novak S, Filipič M (2011) Pre-irradiation of anatase TiO_2 particles with UV enhances their cytotoxic and genotoxic potential in human hepatoma HepG2 cells. J Hazard Mater 196:145–152. doi:10.1016/j.jhazmat.2011.09.004

Schneider OD, Loher S, Brunner TJ, Schmidlin P, Stark WJ (2008) Flexible, silver containing nanocomposites for the repair of bone defects: antimicrobial effect against *E. coli* infection and comparison to tetracycline containing scaffolds. J Mater Chem 18:2679–2684

Schreurs W, Rosenberg H (1982) Effect of silver ions on transport and retention of phosphate by *Escherichia coli*. J Bacteriol 152:7–13

Sotiriou GA, Pratsinis SE (2010) Antibacterial activity of nanosilver ions and particles. Environ Sci Technol 44:5649–5654

Seo JW, Chung H, My Kim, Lee J, Choi Ih, Cheon J (2007) Development of water-soluble single-crystalline TiO_2 nanoparticles for photocatalytic cancer-cell treatment. Small 3:850–853

Thabet S, Weiss-Gayet M, Dappozze F, Cotton P, Guillard C (2013) Photocatalysis on yeast cells: toward targets and mechanisms. Appl Catal B Environ 140–141:169–178. doi:10.1016/j.apcatb.2013.03.037

Thiel J, Pakstis L, Buzby S, Raffi M, Ni C, Pochan DeJ, Shah SI (2007) Antibacterial properties of silver-doped Titania. Small 3:799–803

Wang X, Wu H-F, Kuang Q, Huang R-B, Xie Z-X, Zheng L-S (2009) Shape-dependent antibacterial activities of Ag_2O polyhedral particles. Langmuir 26:2774–2778

Wang D, Zhou Z-H, Yang H, Shen K-B, Huang Y, Shen S (2012) Preparation of TiO_2 loaded with crystalline nano Ag by a one-step low-temperature hydrothermal method. J Mater Chem 22:16306–16311. doi:10.1039/C2JM16217B

Wu D, Long M (2011) Realizing visible-light-induced self-cleaning property of cotton through coating N-TiO_2 film and loading AgI particles. ACS Appl Mater Interfaces 3:4770–4774. doi:10.1021/am201251d

Yamanaka M, Hara K, Kudo J (2005) Bactericidal actions of a silver ion solution on *Escherichia coli*, studied by energy-filtering transmission electron microscopy and proteomic analysis. Appl Environ Microbiol 71:7589–7593

Yang X, Fu H, Yu A, Jiang X (2012) Large-surface mesoporous TiO_2 nanoparticles: synthesis, growth and photocatalytic performance. J Colloid Interface Sci 387:74–83. doi:10.1016/j.jcis.2012.06.080

Yang X, Fu H, Wong K, Jiang X, Yu A (2013) Hybrid Ag@TiO_2 core–shell nanostructures with highly enhanced photocatalytic performance. Nanotechnology 24:415601

YeonáLee H, KunáPark H, MiáLee Y, BumáPark S (2007) A practical procedure for producing silver nanocoated fabric and its antibacterial evaluation for biomedical applications. Chem Commun 28:2959–2961

Zhang L, Xia D, Shen Q (2006) Synthesis and characterization of Ag@TiO_2 core-shell nanoparticles and TiO_2 nanobubbles. J Nanopart Res 8:23–28. doi:10.1007/s11051-005-4883-9

Zhang N, Liu S, Fu X, Xu Y-J (2011) Synthesis of M@TiO_2 (M = Au, Pd, Pt) core-shell nanocomposites with tunable photoreactivity. J Phys Chem C 115:9136–9145. doi:10.1021/jp2009989

Z-m Xiu, Q-b Zhang, Puppala HL, Colvin VL, Alvarez PJ (2012) Negligible particle-specific antibacterial activity of silver nanoparticles. Nano Lett 12:4271–4275